

REVIEW

Open Access



Photocatalytic and electrocatalytic approaches towards atmospheric nitrogen reduction to ammonia under ambient conditions

Jude John[†], Dong-Kyu Lee[†] and Uk Sim^{* ID}

Abstract

Ammonia production is essential for sustaining the demand for providing food for the growing population. Being a great source of hydrogen, it has significant potential in turning out to be a viable candidate for the future hydrogen economy. Ammonia has a high hydrogen content of about 17.6 wt %, is easier to liquefy and is produced in large quantities. Even though large-scale production of ammonia is significant globally, it is used predominantly as a fertilizer. It used also as a transport fuel for vehicles because of its low carbon emissions. Ammonia as an energy storage media is realized in many countries with infrastructure for transportation and distribution already put into place. Currently, the Haber–Bosch process is employed globally in industrial ammonia production and is a high energy expending process requiring large capital investment. In realizing a much economic pathway given the large-scale ammonia production growth forecast, it is necessary to seek new and improved methods for large-scale ammonia production. Amongst them, photoelectrochemical and electrochemical approaches stand as most promising towards nitrogen reduction to ammonia owing to their design features, lesser complexity, and economical in terms of the conventional ammonia production system. Several catalyst materials are investigated which include metal oxides, metals sulfides, carbon-based catalysts, and metal nitrides are all currently being pursued better utilization of their catalytic property towards nitrogen fixation and the minimization of the competing hydrogen evolution reaction (HER). In this article, we have summarized the design and reaction mechanisms for photoelectrochemical and electrochemical nitrogen fixation with the inherent challenges and material-related issues in realizing the Nitrogen Reduction Reaction (NRR).

Keywords: Haber–Bosch process, Nitrogen reduction reaction (NRR), Photoelectrochemical, Electrochemical

1 Introduction

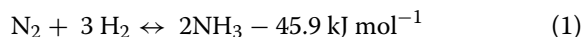
Ammonia (NH₃) synthesis by the Haber–Bosch process is regarded as one of the most significant realizations of the 20th century, contributing to a global production of over 150 million tons of NH₃ yearly, practically 80% of which is in fertilizer production [1]. Global demands for NH₃ production are also likely to increase with its future additional uses such as a carbon-free fuel and particularly as hydrogen storage system owing to its high energy

density (15.3 MJ/L), easy handling and storage [2]. The current system of NH₃ production through the Haber–Bosch process is energy-intensive with global consumption of 1 to 2% of the total annual energy production [3]. The reason for these high level of energy requirements arises from exothermic N₂ reduction reaction as in (1), requires elevated reaction temperatures (~500 °C) and high pressures (>200 atm) and most importantly the need for large volumes of H₂ gas. The potential issue that arises from the usage of natural gas as a source for H₂ is the substantial levels of CO₂ emissions due to its dependence on the natural gas produced through steam reforming [4, 5]. From a thermodynamic standpoint, the NRR

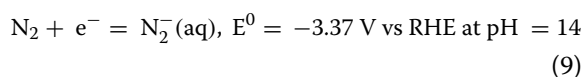
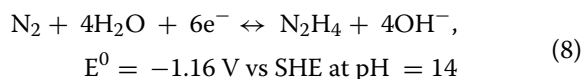
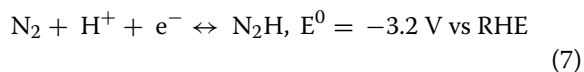
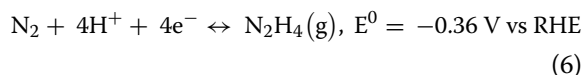
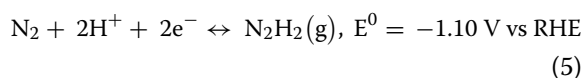
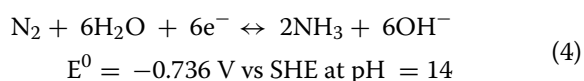
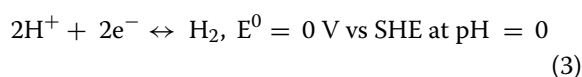
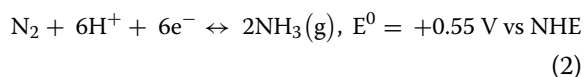
*Correspondence: usim@jnu.ac.kr

[†]Jude John and Dong-Kyu Lee authors contributed equally to this work
Department of Materials Science & Engineering, Chonnam National University, Gwangju 61186, Republic of Korea

is favored much by high pressures and low temperature but in terms of kinetics which requires higher operating temperatures for achieving realistic NH_3 production rates [1].



The fundamental bottleneck in realizing electrochemical reduction of nitrogen can be understood better from the thermodynamic constraints imposed by the intermediate reactions. The NRR equilibrium potentials for different products generated during NRR is as follows:



The electrochemical reduction of N_2 to NH_3 is comparable to H_2 evolution with the following equilibrium potentials. While this is in realizing the fact that H_2 is the main side product during NRR in aqueous electrolytes. Regardless of these NRR takes place via multiple proton-electron transfer reactions, wherein several intermediates are involved. Equation (7) indicates the difficulty in the addition of the first H atom as a much negative redox potential is required. A significantly higher pH for Eq. (8) required for the reaction to compete with Eq. (7). Furthermore, the addition of second H atom is much more complex than the addition of the third H atom, thus requiring a larger reduction potential for the reduction of two-electron and four-electron processes when compared to reduction involving six-electron. (Eqs. (5), (6) and (8)). The thermodynamic difficulty for the N_2 hydrogenation is further clear from the much negative

reduction potentials for the intermediates. Since multiple catalytic reactions associated are with the formation of intermediates, this imposes a much critical limitation to the thermodynamics of NRR [4, 6].

NH_3 besides being used as a fertilizer is currently pursued as a potential energy storage medium analogous to its high hydrogen content compared with that of methanol [7]. NH_3 is expected to play a crucial role in the future hydrogen economy [8]. It is of great importance to developing an environmentally benign method for NH_3 production. Electrocatalytic and photocatalytic approaches are indeed regarded as energy-efficient and offer an environmentally friendly approach towards NH_3 production, as these processes are generally carried out under ambient conditions using solar and wind energy which are renewable energy resources [9]. For example, solar cells and wind turbines can power electrolytic cells for N_2 reduction, and similarly light (photo) driven N_2 reduction can directly access sunlight as a potential light source wherein these two strategies can complement each other for minimizing the carbon emissions by establishing a much realistic NH_3 production compared to the traditional approaches [10, 11]. The sole idea of electrocatalytic and photocatalytic NRR is entirely reliant on catalysts which form the core for the entire NRR [12–14].

Screening of catalysts based on the composition and structure through experimental and theoretical approaches have over time has been done, and many of these electro/photocatalysts have already been designed and fabricated for NH_3 production under ambient conditions [15]. For realizing a suitable electrocatalyst for electrocatalytic NRR, over the past few years, some of the highly researched materials include noble metals, non-noble metals based, and conducting polymer-based electrocatalysts is reported over the past for electrocatalytic NRR operated under ambient conditions. Recently, the focus has shifted towards more potential electrocatalysts including transition metals with flat and stepped surfaces and metal nitrides, which have been explored much in much detail through theoretically calculating the free energy changes after finding the possible intermediates formed on these surfaces [16].

The discovery of TiO_2 as a photocatalytic material for splitting water through irradiating ultraviolet light by Fujishima and Honda completely changed the perspective at which water-splitting viewed in the past [17]. Not until 1977 when Guth and Schrauzer reported that electron-hole pairs were generated by the absorption of light by rutile TiO_2 to reduce N_2 to NH_3 . Here they also required the use of ultraviolet light to excite the photocatalyst [18]. The solar irradiance observed on the earth's surface comprises about 5% ultraviolet radiation (<400 nm), visible light forms 50% (400–800 nm) and lastly infrared light

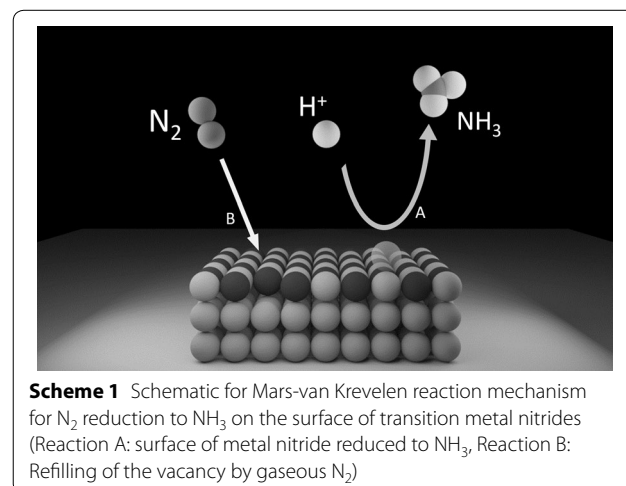
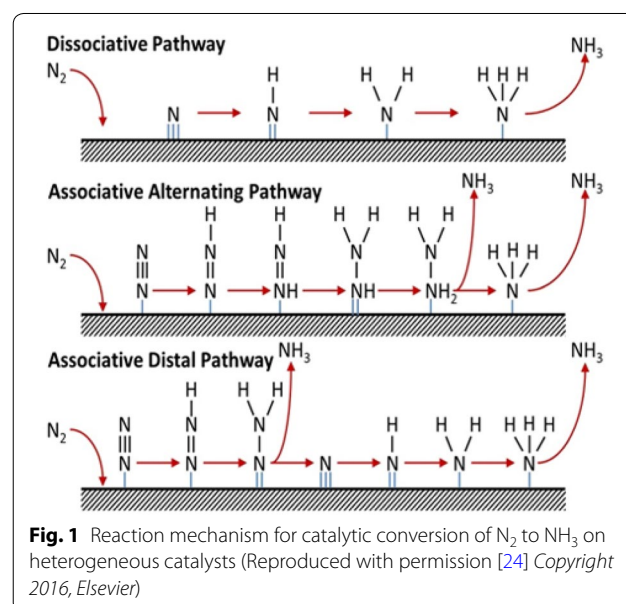
constitutes for almost 45% (> 800 nm). However, the generated NH_3 is oxidized immediately to nitrate making it difficult to generate NH_3 photocatalytically. In the case of photocatalysts, much importance is given specifically to three classes which include inorganic hybrids [19], biomimetic chalcogenides [20], and inorganic semiconductor [21] based electrodes. Among these hydrogen-terminated diamond [22], and black silicon [23] have been employed in the conversion of N_2 to NH_3 under ambient conditions. Electrocatalysts and photocatalysts play vital roles in N_2 fixation to NH_3 , for which we would like to discuss the involved mechanisms. Understanding the underlying mechanism of the NRR is crucial for designing or fabricating efficient catalysts, and with the right knowledge, it would be appropriate to fine-tune or modify the properties of the existing electro/photocatalysts.

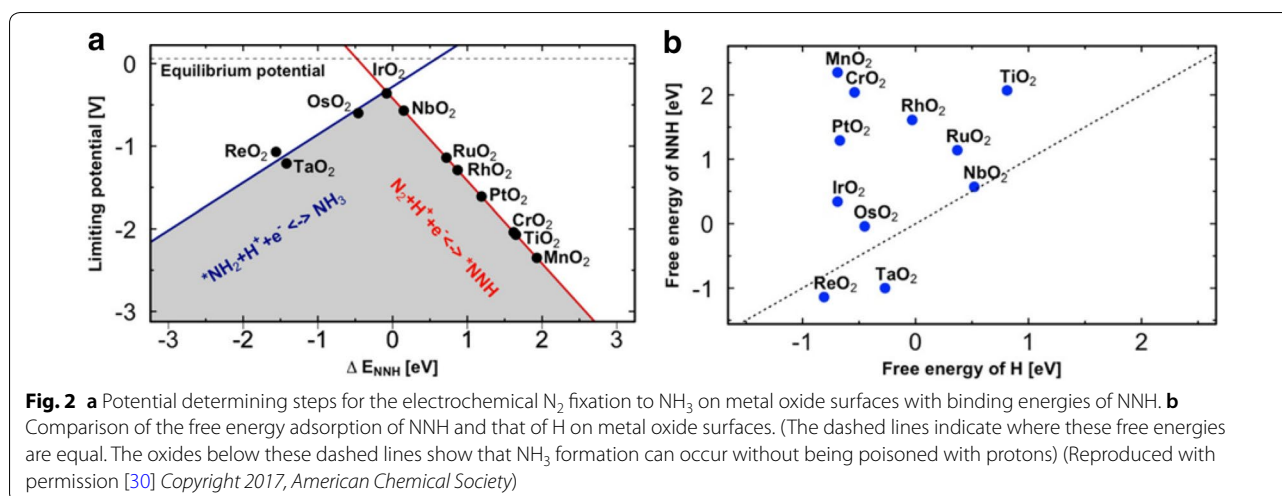
In this review, we would like to address the key reaction mechanisms involved in realizing electrocatalytic and photocatalytic NRR under ambient conditions from a futuristic perspective. We begin by introducing the underlying reactions mechanisms employed for electrocatalytic and photocatalytic N_2 reduction to NH_3 on a heterogeneous catalyst surface. When discussing the reaction mechanisms involved in realizing N_2 reduction to NH_3 , it is necessary to identify the bottlenecks that hinder the natural process. Finally, we list the most promising state-of-the-art electro/photocatalysts reported so far in this area.

2 Reaction mechanisms for electrochemical NRR

The proposed reaction mechanism on a heterogeneous catalyst for the electrochemical N_2 reduction to NH_3 is classified into (1) *associative pathway* and (2) *dissociative pathway* [24]. In *associative pathway*, the N_2 molecule binds to the catalyst surface and further undergoes hydrogenation with the two nitrogen centers bound to each other, and the NH_3 molecule is released after the final $\text{N}\equiv\text{N}$ is broken. The *associative pathway* can be subdivided further into two categories, the *distal pathway* and *alternating pathway* based on different hydrogenation sequences. In *distal pathway* the NH_3 molecule is released after the remote N atom is hydrogenated first, and the hydrogenation process continues further to produce the other NH_3 molecule, while in the *alternating pathway*, the two N atoms are hydrogenated synchronously as shown in Fig. 1 [24]. In the dissociative pathway, the $\text{N}\equiv\text{N}$ bond is broken much before hydrogenation; thus, leaving two adsorbed N-atoms on the catalyst surface. Finally, the adsorbed N atom undergoes independent hydrogenation before conversion to NH_3 . Recently, Abghoui and Skúlason proposed a possible reaction mechanism for N_2 reduction to NH_3 via Mars-van Krevelen (Mvk) as shown in

the Scheme 1, which provides a much favorable reaction mechanism than compared to typical dissociative and associative mechanisms on the surface of transition metal nitride's (TMN) [25]. In the Mvk mechanism for N_2 reduction to NH_3 on TMN, the N atom is reduced to NH_3 , and the catalyst regenerated through the gaseous N_2 while differing from the conventional associative and dissociative mechanism. Further, density functional theory (DFT) calculations revealed that the dissociative mechanism hinders the dissociation of N_2 on the clean surfaces of TMNs is endothermic while the activation barriers being large. The overpotential for N_2 reduction to NH_3 is predicted to be much smaller via the Mvk mechanism than in the case of the associative mechanism [26, 27].





2.1 Principles for designing NRR electrocatalysts

In electrochemical NRR usually, the formation of protons (H^+) occurs at the anode/electrolyte interface. The pivotal step in NRR is the N binding to the catalyst surface and considering this for an ideal electrode material should have an optimized N binding. Various studies conducted on electrochemical NRR on transition metal under ambient conditions report the importance of N binding [28]. A noteworthy point is that with weak binding the catalyst will be unable to activate the reactant, whereas when the binding is firm, there is a possibility that the catalyst being poisoned with the strongly adsorbed intermediates and in turn, creates a volcano-like trend between the bond strength and catalytic activity [16].

These “volcano” diagrams, as displayed in Fig. 2 predict that metals such as Mo, Fe, Rh, and Ru are the most suitable catalyst for NRR activity [16]. However, at the same time, the HER volcano plot also summarizes that these metals are more active for HER than NRR at the same potentials, which reduces the Faradaic efficiency for the NRR while HER is the competing reaction. From the volcano plot, it was found that Mo and Fe to be the most promising candidates for electrochemical N_2 reduction to NH_3 via the associative mechanism. However, another issue is that these active sites on the catalyst surface could be occupied by oxygen rather than N_2 in the presence of water thereby minimizing the efficiency of these catalysts. A recent computational study conducted on Mo nanoclusters shows that the active sites specifically bind oxygen over N_2 and H_2 [29]. It is therefore imperative that much negative potential is required to reduce the oxygen adsorption on the surface and promote N_2 adsorption. The studies conducted for NRR on the surfaces of Ag and Cu with weak N binding showed that it was limited by the adsorption of N_2 as *N_2H as the first

step and protonation of *NH to *NH_2 . However, in case of metals like Re that bind strongly to nitrogen, the removal of *NH_2 to release NH_3 is the limiting step [27]. In the case of noble metals like Pt [16] it has been found that the N-coverage is smaller when compared to H-adatoms at the same onset potential for NH_3 formation, which is indicative of the fact that the HER is the most competing reaction with NRR.

The possibility of N_2 reduction for NH_3 activation under ambient conditions have been recently explored intensively on the (110) facet of several metal oxides [30], of them the most promising candidates turned out to be NbO_2 , ReO_2 , and TaO_2 . Metal nitrides are another class of highly researched materials that show promising results than its metal counterpart towards N_2 reduction to NH_3 than the competing HER. A DFT study performed by Abghoui and Skúlason on TMN surfaces concluded by stating that a suitable catalyst should have high reactivity and stability towards NRR and studies conducted on the surfaces of the mononitrides with Zincblende (ZB) and rocksalt (RS) structures shows that VN, CrN, NbN, ZrN having a rocksalt structure showed lower onset potential for NRR [27].

Among these polycrystalline VN exhibited lower overpotential (-0.5 V) and prevented both HER and catalyst decomposition [27]. 2D materials have also been researched, but these have not been employed much towards NRR. Recently, Azofra et al. [31] implied that 2D transition metal carbides such as MXenes are promising towards N_2 reduction to NH_3 based on DFT calculations. The N_2 chemisorbed on the MXene nanosheets can elongate and weaken the N–N triple bond thereby promoting NRR. Despite these, the critical point to consider while designing an electrocatalyst for efficient NRR is the right material composition, crystal structure, textural structure

(porosity), good electrical conductivity to promote electron transfer, and surface properties which would promote strong affinity towards N-adatoms binding rather than H-adatoms.

2.2 Electrocatalysts for N₂ fixation to ammonia

Electrocatalysts designed for N₂ fixation to NH₃ have been on the rise, and these catalysts could be categorized based on their ability to reduce N₂ to NH₃ under ambient conditions. Here we would like to discuss a few emerging electrocatalysts for NRR. In a recent study, Cui et al. demonstrated that both the NH₃ yield and Faradaic efficiency could be improved by surface modification of hematite nanostructure, with a proof-of-concept wherein hematite electrocatalysts were fabricated with varying concentration of oxygen vacancies (OVs) while annealing in Argon (Ar) and air to modify OV concentration. They were able to achieve better catalytic performance with a higher concentration of OVs. Their *o*-Fe₂O₃-Ar/CNT catalyst produced a maximum NH₃ production rate of 0.46 μg h⁻¹ cm⁻² at -0.9 V vs. Ag/AgCl in 0.1 M KOH electrolyte with a Faradaic efficiency of 6.0%. The durability of the system was further evaluated and was surprisingly able to achieve a high NH₃ production rate of 1.45 μg h⁻¹ cm⁻² with a Faradaic efficiency of 8.28% respectively. This work further elucidates the importance of active sites (oxygen vacancy defects) for N₂ adsorption and activation. Carbon-based materials have received widespread attention in recent years owing to the natural abundance and feasibility in preparation methods. Recently Liu et al. [32] reported the N-doped porous carbon as an efficient electrocatalyst for N₂ fixation to NH₃. N-doped porous carbon showed an enhanced electrocatalytic activity with a high NH₃ production rate of 1.40 mmol g⁻¹ h⁻¹ (-0.9 V) with a maximum current efficiency of 1.42%. The authors believe that the high content of the pyridinic and pyrrolic N might be responsible for promoting the NH₃ formation. DFT studies performed indicate that the preferred pathway for NH₃ formation was through *N≡N→*NH=NH→*NH₂-NH₂→2NH₃. The current study opens up the possibilities of exploring carbon-based materials for NRR under ambient conditions.

Recently Zhang et al. reported MoS₂ as a proof-of-concept for NRR which was theoretically and experimentally confirmed to be active for NRR under ambient conditions. Density functional theory (DFT) calculations performed to study if the MoS₂ edge sites are electrocatalytically active for NRR as it is well known that these edge sites are active for HER. The DFT calculations further performed suggests that the positively charged Mo-edge plays a vital role in polarizing and activating the N₂ molecules. The potential-determining step (PDS) happens to

be the reductive protonation of adsorbed N₂, with a barrier potential of 0.68 eV without any externally applied potential. This relatively low barrier in terms of PDS on Mo-edge further strengthens the claim that MoS₂ as a potential candidate for NRR. Appreciable NH₃ yield of 8.08 × 10⁻¹¹ mol s⁻¹ cm⁻² with a faradaic efficiency of 1.17% respectively. The MoS₂ catalyst exhibited inferior NRR selectivity under acidic conditions than in alkaline conditions, as the electrolyte is infested mostly with protons which would ultimately result in hydrogen evolution. This study offers an exciting new avenue to explore transition metal sulfides as an attractive NRR electrocatalyst for N₂ reduction to NH₃ [33].

Transition metal nitrides-based electrocatalysts have gathered tremendous as they offer an added advantage for the presence of N-adatoms in the crystal structure of the metal atom. Zhang et al. [34] reported the synthesis of MoN nanosheet array as a promising NRR electrocatalyst. They were able to achieve an NH₃ production rate of 3.01 × 10⁻¹⁰ mol s⁻¹ cm⁻² with a Faradaic efficiency of 1.15%. Further DFT calculations proposed that the MoN nanoarray catalyzes NRR via MvK mechanism. This study opened new doors for the rational design of MoN nanocatalysts for efficient NRR.

Another essential breakthrough for the use of TMN catalysts in electrocatalytic NRR recently was proposed by Yang et al. based on Vanadium Nitride nanoparticles as an electrocatalyst for NRR under ambient conditions. They were able to achieve a high NH₃ yield rate of 3.3 × 10⁻¹⁰ mol s⁻¹ cm⁻² with high faradaic efficiency of 6.0% (-0.1 V) in the very first hour of NRR studies. A steady rate of NH₃ production was reported with a yield rate of 1.1 × 10⁻¹⁰ mol s⁻¹ cm⁻² and a Faradaic efficiency of 1.6% even after 116 h. Further studies conducted provided elucidative results that the electrochemical NRR proceeded via MvK mechanism. This was supported through ¹⁵N₂ isotope tests. Combined with the ex situ and operando studies that the surface of VN_{0.7}O_{0.45} is the active phase for electrochemical NRR and the conversion to VN would result in deactivation of the catalyst. This hypothesis is supported also by the DFT studies performed [35].

Song et al. reported N-doped Carbon Nanospikes (CNS) as an efficient electrocatalyst for efficient N₂ fixation to NH₃. The proposed mechanism for the reaction depends on the physical interactions on the sharp surface of the catalyst in the absence of a transition metal on CNS. This mechanism was supported by a control experiment performed with an O-etched CNS where the blunt tips produced small fractions of NH₃ under the same conditions. They were able to achieve a maximum yield of 97.18 μg h⁻¹ cm⁻² with high Faradaic efficiency of 11.56%. The study also stressed on the importance

of counterions in the aqueous electrolyte in enhancing the NH_3 production rates in the order of $\text{Li}^+ > \text{Na}^+ > \text{K}^+$ wherein these small counterions increased the N_2 concentration within the Stern layer. H_2 evolution was suppressed with the formation of the dehydrated cation layer surrounding the tip while minimizing the access to water molecules and allowing access to N_2 molecules in a high electric field. Although this theory requires further elucidation to fully understand this reaction mechanism, which includes the energy needed for the injection of N_2 and the solvation of N_2 and both the counterions. This study provides a viable physical reaction mechanism for electrolysis of N_2 to NH_3 [36].

Nanoscale confinement is a crucial aspect of improving N_2 selectivity on the electrocatalysts surface. Recently Nazemi et al. reported the electrosynthesis of NH_3 from N_2 and water under ambient conditions with hollow gold nanocages (AUHNCs) as the catalyst. The significant findings from this study are the interdependency of the Ag content in the interior of the Au hollow nanoparticles, pore size/density and finally, the total surface area of the nanoparticles contributed for the enhanced electrocatalytic activity for NRR. Another important finding was the presence of Ag in the cavity of AuHNCs-635 was found to decrease the electrocatalytic activity towards NRR as Ag enhances H_2 evolution. Among the various shapes tested for NRR AuHNCs with Localized surface plasmon resonance (LSPR) value of 715 showcased highest NH_3 yield rates of $3.74 \mu\text{g cm}^{-2} \text{h}^{-1}$ and high Faradaic efficiency of 35.9% was achieved at -0.4 V vs. RHE. The higher FE and NH_3 yield rates of AuHNCs-715 resulted from the better selectivity for N_2 reduction as the pore size, Ag content in the cavity and the active surface area of the nanoparticle played a crucial role in enhancing N_2 selectivity. As primarily NRR happens in the cavities of AuHNCs, a smaller pore didn't enhance the N_2 selectivity as a higher Ag content resulted in lower selectivity with increased H_2 evolution. Further increase in pore size results in decreased NRR selectivity due to the decreased surface area and lack of confinement of the reactants within the cavities (AuHNCs-795). Compared to AuHNCs with larger pore size but do not have Ag in the cavities. Further increase in pore size results in decreased NRR selectivity due to the decreased surface area and lack of confinement of the reactants within the cavities (AuHNCs-795) [37].

Recently Yao et al. reported the use of Chromium Oxynitride ($\text{CrO}_{0.66}\text{N}_{0.56}$) as an efficient electrocatalyst for N_2 fixation to NH_3 using a homemade proton exchange membrane electrolyzer (PEMEL) under ambient conditions. A high NH_3 yield rate of $8.9 \times 10^{-11} \text{ mol s}^{-1} \text{ cm}^{-2}$ with high Faradaic efficiency of 6.7% was achieved at 2.0 and 1.8 V respectively. The NRR activity

of $\text{CrO}_{0.66}\text{N}_{0.56}$ is better than pure Cr_2O_3 and CrN catalysts. The study also provided more insights into the improved electronic properties of metal nitrides through partial oxidation which opens the door towards designing rational electrocatalysts for NRR [38].

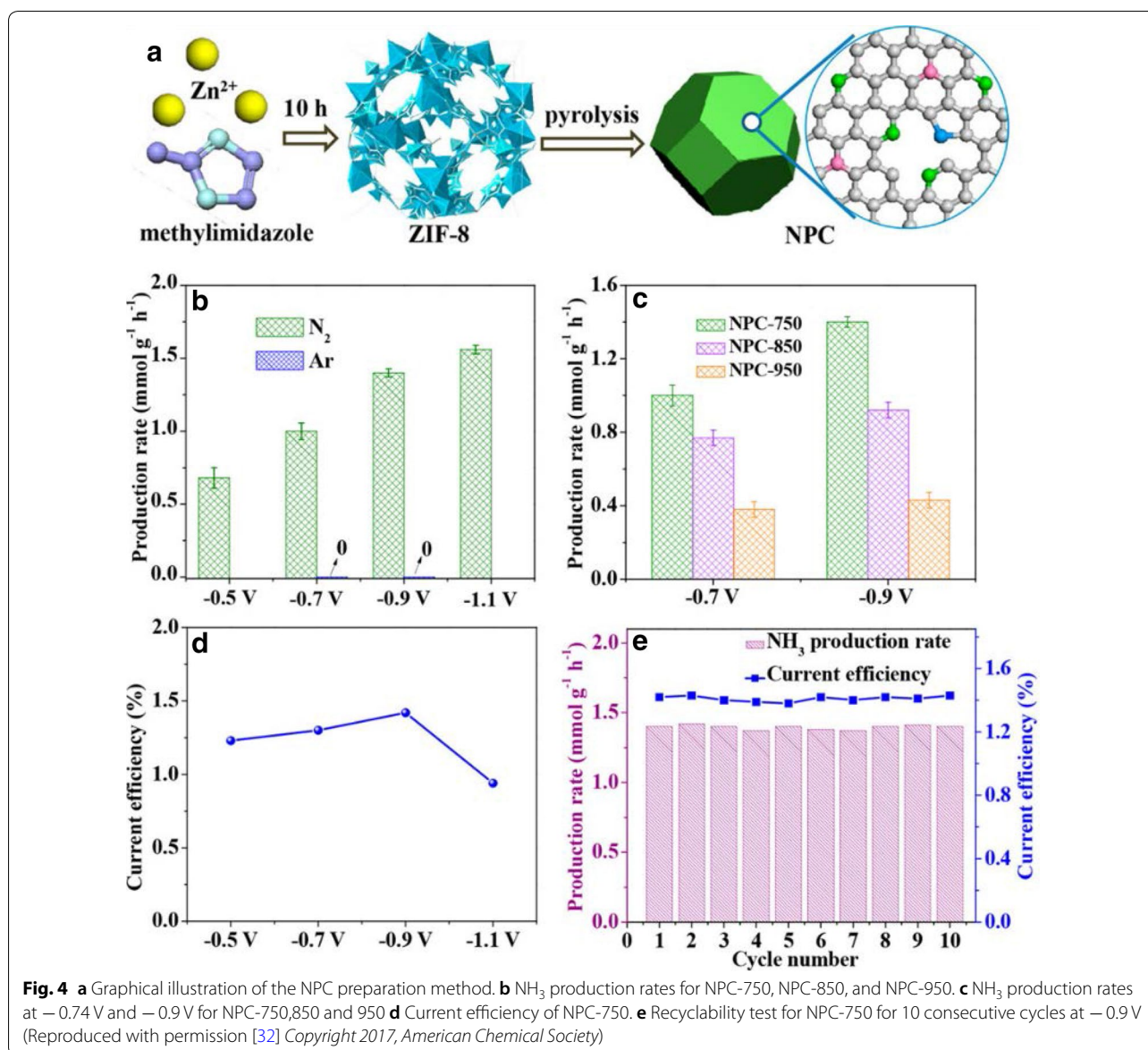
3 Reaction mechanism for photocatalytic NRR

Photocatalytic N_2 reduction to NH_3 typically follows several steps before the release of the NH_3 molecule. The first step involves the occupation of the conduction band by the photogenerated electrons which leaves behind a vacancy in the valance band that will be occupied by holes. Subsequently, some these photogenerated electrons and holes recombine while some drift to the surface of the catalyst and take part in the redox reactions on the surface. At this point, H_2O can be oxidized to O_2 by the holes whereas N_2 reduced to NH_3 after a series of multiple generations of electrons and water-derived protons [39, 40].

A well-known fact regarding photocatalytic redox reaction is that it is entirely reliant on the reduction potential of the adsorbate and band position of the semiconductor electrode [41–43]. For instance, it is necessary that the position of the conduction band of a semiconductor electrode should be higher (more negative) in relative to the reduction potential required for N_2 hydrogenation, while the valance band position is located much lower (more positive) for oxygen evolution potential [44–46]. This leads to limitations which mainly revolves around two aspects one being the ability to active N_2 molecule for NH_3 formation. This also requires developing semiconductor electrodes with small bandgap preferably along the visible light region, which would still fulfill the necessary thermodynamic conditions for the reduction of N_2 to NH_3 . The second limitation is the necessity to suppress the recombination of the charge carriers to obtain a higher solar conversion efficiency and apparent quantum yield for the reaction [46].

3.1 Design principles for photocatalytic NRR

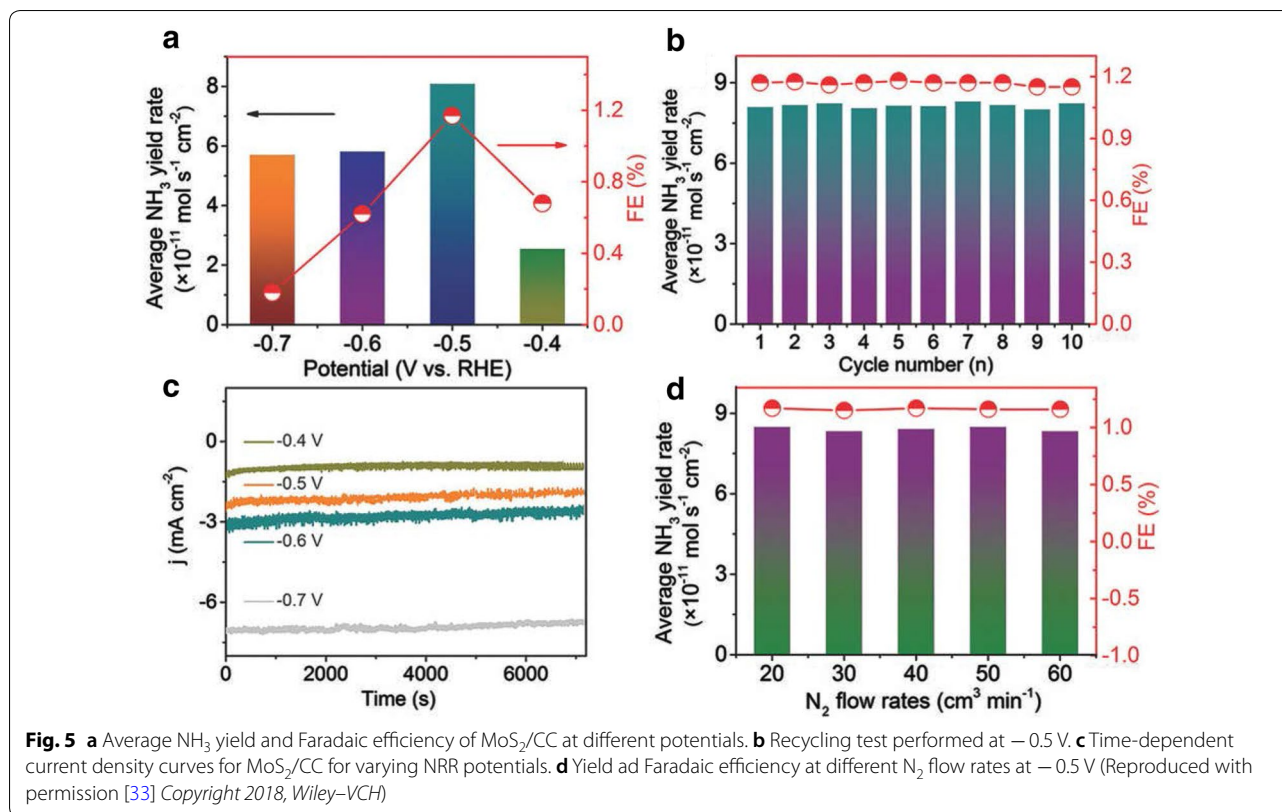
Several recent investigations carried out from the experimental and theoretical viewpoint on the N_2 reduction mechanisms over various photocatalysts [31, 47, 48]. For a better understanding of the N_2 reduction to NH_3 especially on hydrogenation on photocatalysts it is necessary to understand the process in greater detail. For instance, in the first photogenerated electron transfer, the N_2 adsorbed on the catalyst surface attains a proton (H^+) from the environment and a photogenerated electron from the catalyst to generate the necessary chemical species. Photocatalytic N_2 fixation differs from conventional N_2 reduction on transition metals because the former is a chemical process occurring on a semiconductor surface.



lattice promotes better electron transfer to N_2 molecules. Mo-doping introduces an elevation of the defect band center towards the Fermi level which generates more energy into the photoexcited electrons for N_2 fixation to NH_3 [52].

Yang et al. reported nitrogen photofixation using plasmonic gold nanocrystal on ultrathin nanosheets. Based on the “working-in-tandem” concept of natural nitrogenase herein they have constructed a N_2 photofixation system comprising of inorganic Au/ TiO_2 -OV catalysts. The oxygen vacancies (OVs) acted as the activation sites for N_2 molecules, whereas the plasmonic electrons acting

as the reducing agents for the final fixation of the N_2 to NH_3 . Au/ TiO_2 -OV catalyst exhibited a high NH_3 yield of $130.5 \text{ mmol h}^{-1} \text{ g}^{-1}$ with an apparent quantum efficiency of 0.82% at 550 nm. The authors reported that the “working-in-tandem” strategy effectively tackles two important criteria for activation and reduction of N_2 to form NH_3 . Thus, optimizing the absorption across the overall visible range with the mixture of Au nanospheres and nanorods which further elevates the N_2 photofixation rate by 66.2% in comparison with the Au nanospheres solely [53] Tables 1 and 2 describes a brief summary on the representative NRR photocatalysts and electrocatalysts.



4 Strategies for improving selectivity towards N_2 fixation to NH_3

Current systems for NRR lack efficient electro/photocatalyst for N_2 reduction to NH_3 . Most of the catalysts reported so far are limited in terms of the large overpotential required for N_2 reduction to NH_3 and the low faradaic efficiencies of these systems are major concerns. The thermodynamics of NRR suggest that the reaction should proceed towards negative potentials wherein HER is more influenced this raises the question of selectivity. The other factors that affect N_2 reduction to NH_3 lies in the electrode material, conductivity of the catalyst material, electrolyte used, operating conditions (temperature), and applied potential.

The intrinsic reactivity can be enhanced by incorporating various strategies which include effects of crystal facets, [54, 55] size effects, [56] and amorphous nature of the catalyst, [57] have been found to be very decisive for

electro/photocatalytic NRR. As discussed earlier limiting the availability of protons or electrons at the surface of the catalysts is another important aspect to suppress HER and provide selectivity towards NRR. Many strategies have been explored and recently to limit the concentration in the solution researchers have made use of mixture of electrolytes for aqueous based systems [58]. It is also very important to validate that the origin of NH_3 produced from N_2 is appropriately quantified using experiments such as $^{15}\text{N}_2$ reduction and measured using $^1\text{H-NMR}$. Finally, the electron transfer rate at the interface between the current collector and active material and the interface between the electrode and electrolyte can also play an important role in minimizing HER and showing selectivity towards NRR. One must also take into consideration the underlying drawbacks that needs to be dealt while trying to limit the electron transfer rate towards HER as would result in lesser faradaic

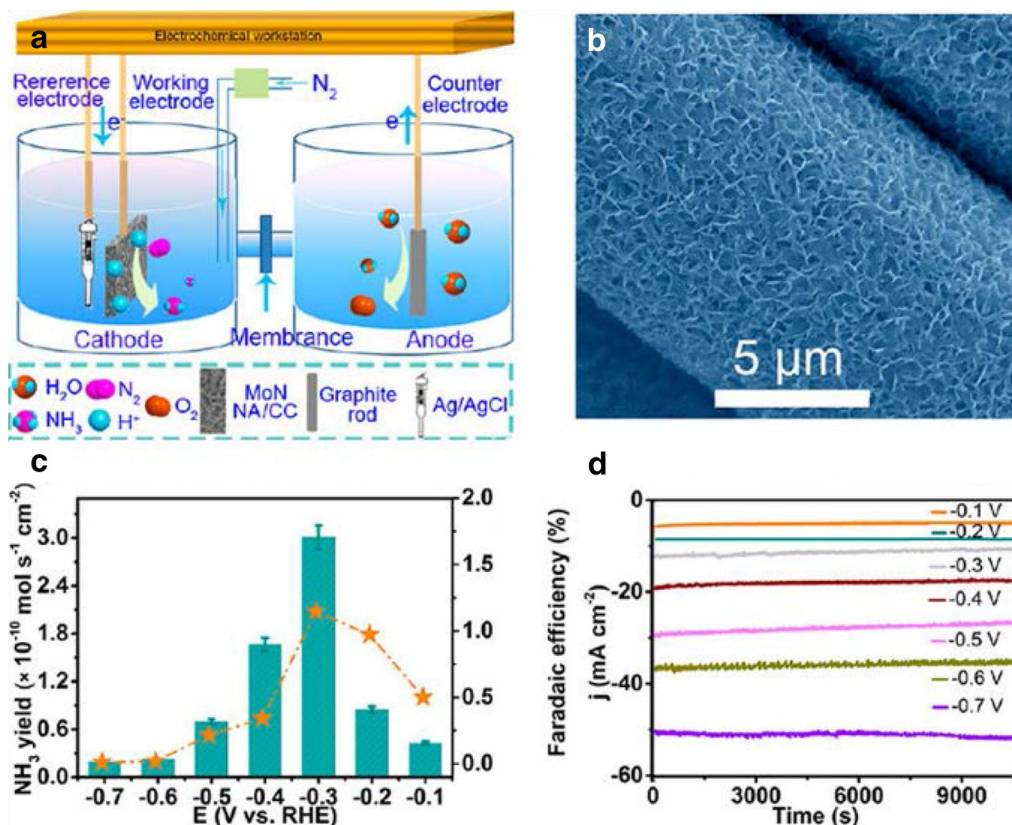


Fig. 6 **a** Schematic illustration for electrocatalytic NRR. **b** SEM image showing MoN NA/CC. **c** NH_3 yields and FE at different potentials. **d** Chronoamperometry results at various potentials (Reproduced with permission [34] Copyright 2018, American Chemical Society)

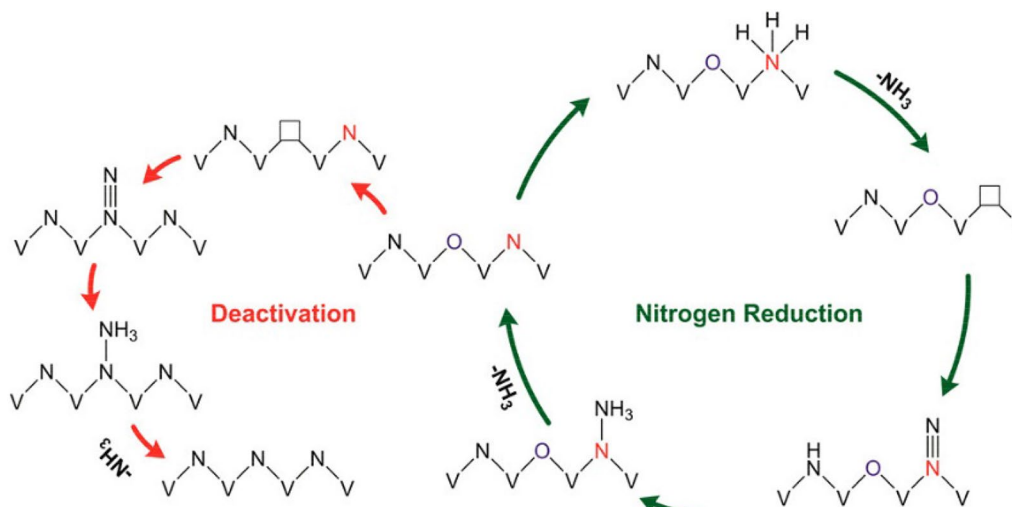


Fig. 7 The proposed reaction pathway for N_2 reduction on $\text{VN}_{0.7}\text{O}_{0.45}$ via MvK mechanism and the deactivation of the catalyst (Reproduced with permission [35] Copyright 2018, American Chemical Society)

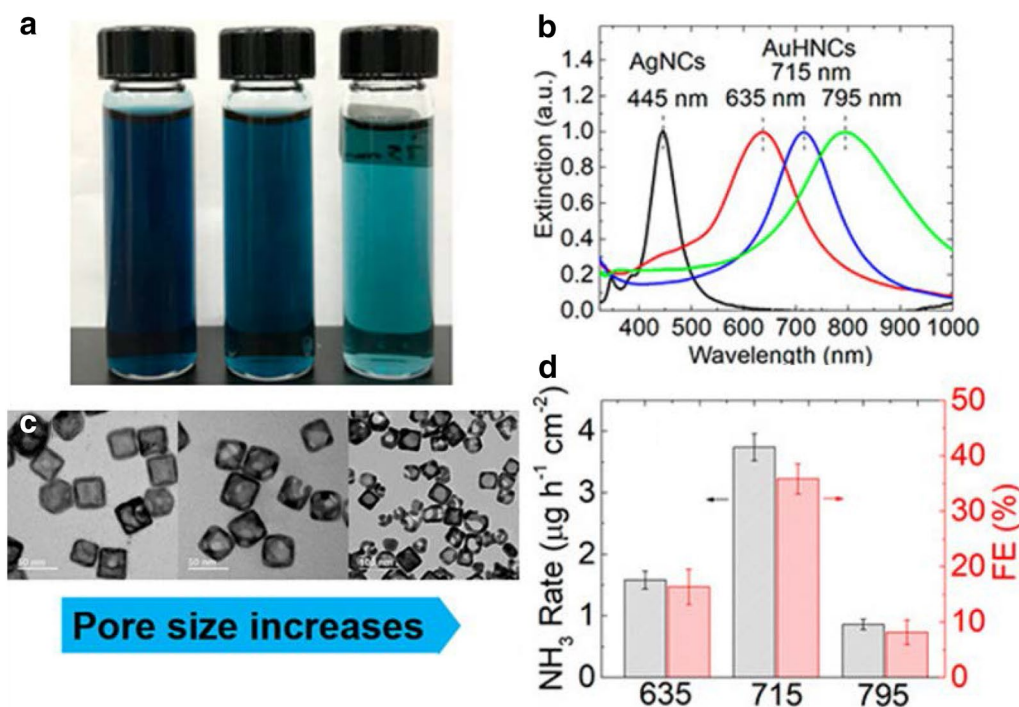


Fig. 8 **a** AuHNCs dispersed in DI water. **b** UV-vis spectra of AgNCs and AuHNCs with various peak LSPR values. **c** TEM images displaying AuHNCs with peak LSPR at 635, 715 and 795 nm. **d** NH₃ yield rate and Faradaic efficiency for the various LSPR peak values at -0.4 V (Reproduced with permission [37] Copyright 2018, American Chemical Society)

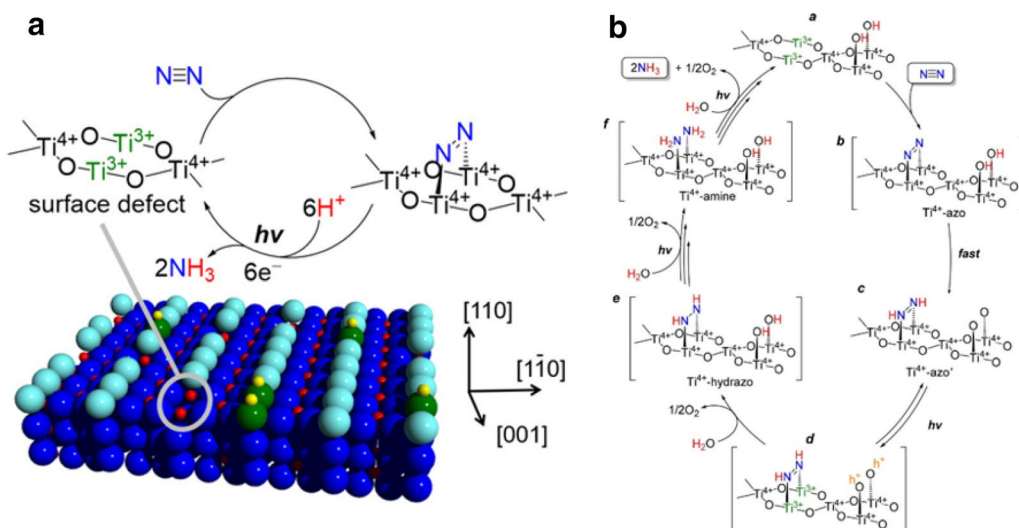


Fig. 9 **a** Photocatalytic N₂ fixation on the surface of Rutile TiO₂ (110) surface. **b** The mechanism for the photocatalytic fixation of N₂ to NH₃ over the surface oxygen vacancies of TiO₂ (Reproduced with permission [49] Copyright 2017, American Chemical Society)

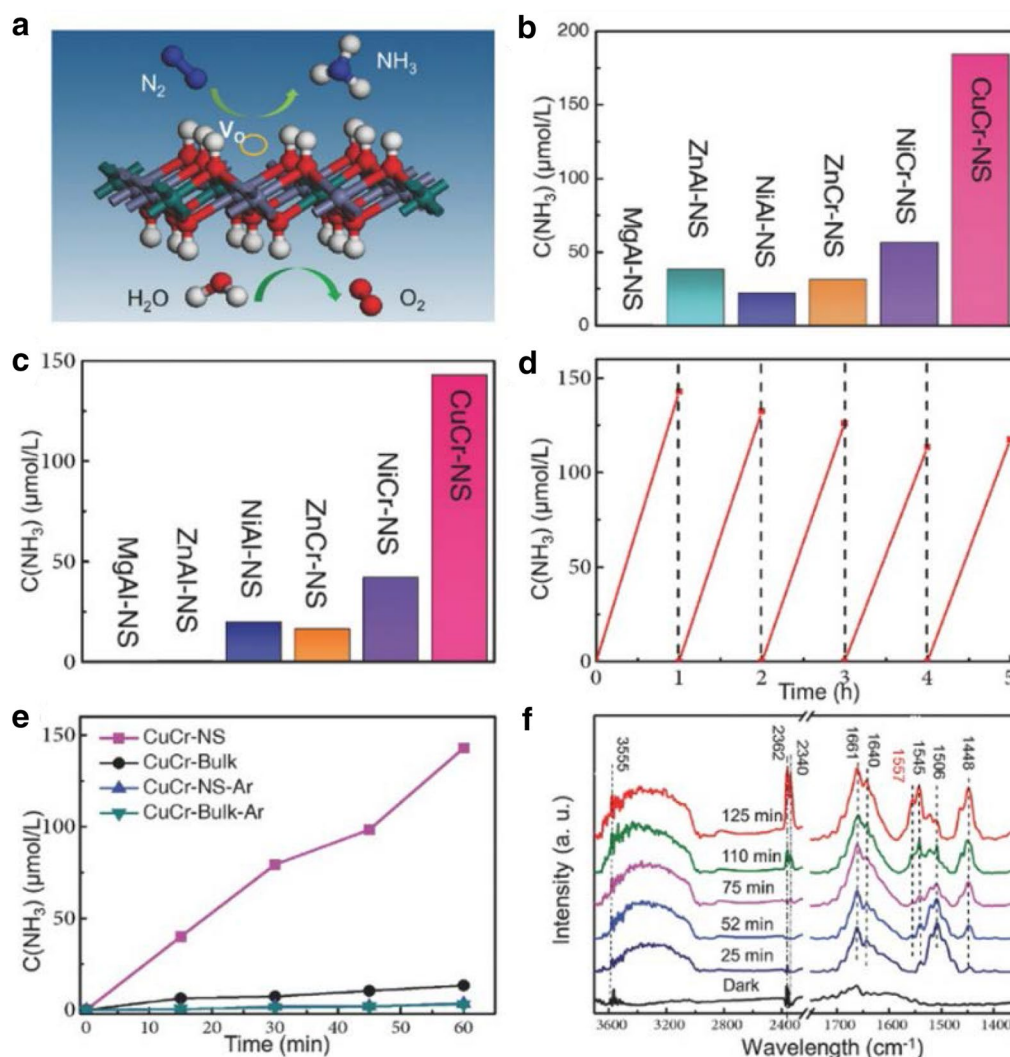


Fig. 10 **a** Illustration of the N_2 fixation process. **b, c** NH_3 yield over a 1 h test period on different LDH photocatalysts with UV-vis illumination. **d** Catalyst stability tests performed for CuCr-NS in N_2 under visible-light illumination. **e** Time-dependent NH_3 evolution under N_2 and Ar. **f** In situ IR spectra recorded for CuCr-NS under N_2 during 125 min UV-vis illumination (Reproduced with permission [50] Copyright 2017 Wiley-VCH)

efficiencies of the system. It would be therefore astute to have an optimum balance between selectivity to attain a higher performance.

5 Conclusion

In summary, we have discussed the advancement in electro/photocatalytic NRR and the underlying theoretical and experimental progress so far. Despite all

the challenges and obstacles ahead we believe electro/photocatalytic NRR is much more realizable with its current growth. Moreover, in the near future, theoretical and experimental advancement coupled with operando/in situ studies will further shift the tide in developing much efficient electro/photocatalysts which

Table 1 A brief summary of the representative experimental studies on NRR using various electrocatalytic heterogeneous catalysts

Catalyst	Electrolyte	Condition	NH ₃ formation rate	Unit	Potential	Reference electrode	Faradaic efficiency	Year
Fe-phthalocyanine	1.0 M KOH	25 °C	7.0E+05	mol s ⁻¹ cm ⁻²	-47.8 mA cm ⁻²	Current density	0.34%	1989 [59]
ZnS	1.0 M KOH	25 °C	7.1E+06	mol s ⁻¹ cm ⁻²	-0.1 V	vs RHE	0.964%	1990 [60]
ZnSe	1.0 M KOH	25 °C	8.1E+06	mol s ⁻¹ cm ⁻²	-0.1 V	vs RHE	1.29%	1990 [60]
Ti	0.2 M LiClO ₄ /0.18 M ethanol in THF	25 °C			2.0 V	Cell Voltage	8.20%	1994 [60]
Cu	0.2 M LiClO ₄ /0.18 M ethanol in THF	25 °C			2.0 V	Cell Voltage	5.30%	1994 [61]
Ru/C	2.0 M KOH	20 °C	3.43137E-12	mol s ⁻¹ cm ⁻²	-1.10 V	vs Ag/AgCl	0.28%	2000 [62]
		90 °C	4.08497E-12	mol s ⁻¹ cm ⁻²	-0.96 V	vs Ag/AgCl	0.92%	2000 [62]
Polyaniline	methanol/LiClO ₄ /H ₂ SO ₄	25 °C	0.000,000,014	mol ⁻¹ ml ⁻¹	-0.12 V	vs RHE	2.00%	2005 [63]
30 wt % Pt/C	0.50 M H ₂ SO ₄	RT	1.14E-09	mol s ⁻¹ cm ⁻²	1.6 V	Cell Voltage	0.50%	2013 [64]
	H ⁺ /Li ⁺ /NH ₄ ⁺ mixed electrolyte	80 °C	9.37E-10	mol s ⁻¹ cm ⁻²	1.2 V	Cell Voltage	0.83%	2013 [65]
Ru/Ti	0.50 M H ₂ SO ₄	30 °C	1.2E-10	mol s ⁻¹ cm ⁻²	-0.15 V	vs NHE	N/A	2014 [66]
Rh/Ti			1.5E-11	mol s ⁻¹ cm ⁻²	-0.171 V			
Ni wire	0.050 M H ₂ SO ₄ /0.1 M LiCl/EDA	RT	3.58E-11	mol s ⁻¹ cm ⁻²	1.8 V	Cell Voltage	17.20%	2016 [58]
Porous Ni	2-propanol/H ₂ SO ₄	RT	1.54E-11	mol s ⁻¹ cm ⁻²	0.5 mA cm ⁻²	Current Density	0.89%	2016 [67]
Mo nanofilm	0.010 M H ₂ SO ₄	RT	3.09E-11	mol s ⁻¹ cm ⁻²	-0.49 V	vs RHE	0.72%(at -0.29 V vs RHE)	2017 [54]
γ-Fe ₂ O ₃	0.10 M KOH	65 °C	1.21528E-11	mol s ⁻¹ cm ⁻²	0 V	vs RHE	1.96%	2017 [68]
Au nanorods	0.10 M KOH	RT	2.69281E-11	mol s ⁻¹ cm ⁻²	-0.2 V	vs RHE	4.00%	2017 [55]
Au/TiO ₂	0.10 M HCl	RT	3.49673E-10	mol s ⁻¹ mg _{cat} ⁻¹	-0.2 V	vs RHE	8.11%	2017 [56]
Au-CeOx/RGO	0.10 M KOH	RT	1.35621E-10	mol s ⁻¹ mg _{cat} ⁻¹	-0.2 V	vs RHE	10.10%	2017 [57]
30 wt % Fe ₂ O ₃ -CNT	0.50 M KOH	RT	6.74E-12	mol s ⁻¹ cm ⁻²	-2.0 V	vs Ag/AgCl	0.16%	2017 [69]
PEBCD (poly N-ethyl-benzene-1,2,4,5-tetracarboxylic diimide)/C	0.50 M Li ₂ SO ₄	25 °C	2.5817E-11	mol s ⁻¹ cm ⁻²	-0.5 V	vs RHE	2.85%	2017 [70]
		40 °C	7.07516E-11	mol s ⁻¹ cm ⁻²	-0.5 V		4.87%	
MOF(Fe)(metal-organic-frameworks)	2.0 M KOH	90 °C	2.12E-09	mol s ⁻¹ cm ⁻²	1.2 V	Cell Voltage	1.43%	2017 [71]
Fe ₂ O ₃ -CNT	2.0 M NaHCO ₃	RT	3.59477E-12	mol s ⁻¹ cm ⁻²	-2.0 V	vs Ag/AgCl	0.15%(at -1.0 V vs Ag/AgCl)	2017 [72]
Fe on stainless steel mesh	ionic liquid	RT	3.88889E-10	mol s ⁻¹ cm ⁻²	-0.8 V	vs NHE	30%	2017 [73]
N-doped carbon	0.05 M H ₂ SO ₄	RT	3.88889E-16	mol s ⁻¹ mg ⁻¹	-0.9 V	vs RHE	1.42%	2018 [32]
Ru nanosheets	0.10 M KOH	RT	3.90196E-10	mol s ⁻¹ mg _{cat} ⁻¹	-0.2 V	vs RHE	0.217%	2018 [74]
Mo ₂ N nanorod	0.1 M HCl	25 °C	1.28105E-09	mol s ⁻¹ mg _{cat} ⁻¹	-0.3 V	vs RHE	4.50%	2018 [75]
VN nanowire array	0.1 M HCl	25 °C	2.48E-10	mol s ⁻¹ cm ⁻²	-0.3 V	vs RHE	3.58%	2018 [76]
Pt	6 M KOH/polymer gel	30 °C	4.049E-11	mol s ⁻¹ cm ⁻²	0.5 V	Cell Voltage	0.0108%	2018 [77]
Ir		60 °C	2.763E-11	mol s ⁻¹ cm ⁻²	0.25 V	Cell Voltage	0.108%	
Bi ₄ V ₂ O ₁₁ /CeOx	HCl, PH=1	RT	3.79248E-10	mol s ⁻¹ mg _{cat} ⁻¹	-0.2 V	vs RHE	10.16%	2018 [78]

Table 1 (continued)

Catalyst	Electrolyte	Condition	NH ₃ formation rate	Unit	Potential	Reference electrode	Faradaic efficiency	Year
Pore-size-controlled hollow gold nanocatalysts	0.1 M LiOH	RT	6.1111E-11	mol s ⁻¹ cm ⁻²	-0.4 V	vs RHE	35.90%	2018 [37]
Hollow gold nanocages	0.5 M LiClO ₄	RT	6.37255E-11	mol s ⁻¹ cm ⁻² at -0.5 V	-0.4 V	vs RHE	30.20%	2018 [79]
MoN Nanosheets	0.1 M HCl	RT	3.01	mol s ⁻¹ cm ⁻²	-0.3 V	vs RHE	1.15%	2018 [34]
N-doped carbon nanospikes	0.25 M LiClO ₄	RT	1.58791E-09	mol s ⁻¹ cm ⁻²	-1.19 V	vs RHE	11.56 ± 0.85%	2018 [36]
Vanadium Nitride Nanoparticles	3 M KOH	RT	3.31E-10	mol s ⁻¹ cm ⁻²		vs RHE	5.95%	2018 [35]
Chromium Oxynitride nanoparticles	Nafion Solution(5% wt)	RT	8.9E-11	mol s ⁻¹ cm ⁻²	2.0 V	Cell Voltage	6.70%	2018 [38]
MoS ₂	0.1 M Na ₂ SO ₄	RT	8.08E-11	mol s ⁻¹ cm ⁻²	-0.5 V	vs RHE	1.17%	2018 [33]

Table 2 A brief summary of the representative experimental studies on NRR using various photocatalytic heterogeneous catalysts

Catalyst	Electrolyte	Condition	NH ₃ formation rate	Unit	Quantum efficiency	Light source	Year
FeMoS-chalcogels	Pyridinium hydrochloride and sodium ascorbate	25 °C	4.44E-11	mol s ⁻¹	N/A	150 W Xenon Lamp	2015 [20]
BiOBr nanosheets	Water	25 °C	2.89E-08	mol s ⁻¹ g ⁻¹	0.23%	Visible Light (λ > 420 nm)	2015 [21]
Graphitic carbon nitride(g-C ₃ N ₄)	0.1 M Na ₂ SO ₄	RT	3.44444E-07	mol s ⁻¹ g ⁻¹	N/A	300 W Xe lamp (λ > 420 nm)	2015 [51]
CdS:nitrogenase MoFe protein biohybrid	0.5 M HEPES	25 °C	5.25E-06	mol s ⁻¹ g ⁻¹	3.30%	~3.5 mW cm ⁻² of 405 nm	2016 [19]
Titanium dioxide	Water	RT	1.01273E-09	mol s ⁻¹ g ⁻¹	0.02% (Solar to chemical energy)	1sun	2017 [49]
CuCr-LDH(Layered-Double-Hydroxide) Nanosheets	1 M KOH	25 °C	1.85E-04	mol L ⁻¹	N/A	300 W Xe lamp (λ > 400 nm)	2017 [50]
Bi ₂ WO ₆ by cyclized polyacrylonitrile (c-PAN)	Water	RT	3.89E-08	mol s ⁻¹ g ⁻¹	N/A	visible light provided by a 300 W Xe lamp	2018 [80]
Mo-doped W ₁₈ O ₄₉ ultrathin nanowires	0.5 M Na ₂ SO ₄	RT	5.43E-08	mol s ⁻¹ g _{cat} ⁻¹	0.33%	300 W Xe lamp	2018 [52]
Au nanocrystal-decorated ultrathin TiO ₂ nanosheets	Water and Methanol		3.63E-08	mol s ⁻¹ g ⁻¹	0.82%	300 W Xe lamp (λ > 420 nm)	2018 [53]
ECG (electrochemical grade) boron-doped diamond	Water	25 °C	5.55556E-11	mol s ⁻¹	N/A	450 W high-pressure Hg/Xe lamp (λ > 180 nm)	2013 [22]
Plasmon-enhanced black silicon	SO ₃ ²⁻ Solution	25 °C	2.12418E-09	mol s ⁻¹ cm ⁻²	0.003%	2suns	2018 [23]

much higher selectivity towards N₂ reduction for NH₃ formation.

Authors' contributions

JJ, DKL, and US contributed to this work in manuscript preparation. The authors have read and approved the final manuscript.

Competing interests

The authors declare that they have no competing interests.

Availability of data and materials

The review is based on the published data and sources of data upon which conclusions have been drawn can be found in the reference list.

Funding

This work has supported by the National Research Foundation of Korea (NRF) grant funded by the Korea government (No. 2018R1C1B60012167 and 2018R1A5A1025224).

Publisher's Note

Springer Nature remains neutral with regard to jurisdictional claims in published maps and institutional affiliations.

Received: 17 January 2019 Accepted: 18 March 2019

Published online: 25 April 2019

References

- J.N. Galloway, A.R. Townsend, J.W. Erisman, M. Bekunda, Z. Cai, J.R. Freney, L.A. Martinelli, S.P. Seitzinger, M.A. Sutton, *Science* **320**(5878), 889–892 (2008)
- Appl, M.J.F. NH₃ principles and industrial practice. **245**, 12 (1999)
- H. Liu, *Chin. J. Catal.* **35**(10), 1619–1640 (2014)
- C.J. Van der Ham, M.T. Koper, D.G. Hettterscheid, *Chem. Soc. Rev.* **43**(15), 5183–5191 (2014)
- Y. Tanabe, Y. Nishibayashi, *Coord. Chem. Rev.* **257**(17–18), 2551–2564 (2013)
- S.G. Bratsch, *J. Phys. Chem. Ref. Data* **18**(1), 1–21 (1989)
- R. Lan, J.T. Irvine, S. Tao, *Int. J. Hydrogen Energy* **37**(2), 1482–1494 (2012)
- C.H. Christensen, T. Johannessen, R.Z. Sørensen, J.K. Nørskov, *Catal. Today* **111**(1–2), 140–144 (2006)
- K. Sun, I.A. Moreno-Hernandez, W.C. Schmidt, X. Zhou, J.C. Crompton, R. Liu, F.H. Saadi, Y. Chen, K.M. Papadantonakis, N.S. Lewis, *Energy Environ. Sci.* **10**(4), 987–1002 (2017)
- RF Service, *Science* **345**(6197), 610 (2014)
- T. Oshikiri, K. Ueno, H. Misawa, *Angew. Chem.* **128**(12), 4010–4014 (2016)
- H.P. Jia, E.A. Quadrelli, *Chem. Soc. Rev.* **43**(2), 547–564 (2014)
- Y.P. Zhu, C. Guo, Y. Zheng, S.Z. Qiao, *Acc. Chem. Res.* **50**(4), 915–923 (2017)
- M. Yue, R. Wang, N. Cheng, R. Cong, W. Gao, T. Yang, *Sci. Rep.* **6**, 30992 (2016)
- L.M. Duman, W.S. Farrell, P.Y. Zavalij, L.R. Sita, *J. Am. Chem. Soc.* **138**(45), 14856–14859 (2016)
- E. Skulason, T. Bligaard, S. Gudmundsdóttir, F. Studt, J. Rossmeisl, F. Abild-Pedersen, T. Vegge, H. Jonsson, J.K. Nørskov, *Phys. Chem. Chem. Phys.* **14**(3), 1235–1245 (2012)
- A. Fujishima, K. Honda, *Nature* **238**(5358), 37 (1972)

18. G.N. Schrauzer, T.D. Guth, *J. Am. Chem. Soc.* **99**(22), 7189–7193 (2002)
19. K.A. Brown, D.F. Harris, M.B. Wilker, A. Rasmussen, N. Khadka, H. Hamby, S. Keable, G. Dukovic, J.W. Peters, L.C. Seefeldt, P.W. King, *Science* **352**(6284), 448–450 (2016)
20. A. Banerjee, B.D. Yuhas, E.A. Margulies, Y. Zhang, Y. Shim, M.R. Wasielewski, M.G. Kanatzidis, *J. Am. Chem. Soc.* **137**(5), 2030–2034 (2015)
21. H. Li, J. Shang, Z. Ai, L. Zhang, *J. Am. Chem. Soc.* **137**(19), 6393–6399 (2015)
22. D. Zhu, L. Zhang, R.E. Ruther, R.J. Hamers, *Nat. Mater.* **12**(9), 836 (2013)
23. M. Ali, F. Zhou, K. Chen, C. Kotzur, C. Xiao, L. Bourgeois, X. Zhang, D.R. MacFarlane, *Nat. Commun.* **7**, 11335 (2016)
24. M.A. Shipman, M.D. Symes, *Catal. Today* **286**, 57–68 (2017)
25. Y. Abghoui, A.L. Garden, V.F. Hlynsson, S. Björgvinsdóttir, H. Ólafsdóttir, E. Skúlason, *Phys. Chem. Chem. Phys.* **17**(7), 4909–4918 (2015)
26. Y. Abghoui, E. Skúlason, *Catal. Today* **286**, 69–77 (2017)
27. Y. Abghoui, A.L. Garden, J.G. Howalt, T. Vegge, E. Skúlason, *ACS Catal.* **6**(2), 635–646 (2015)
28. J.H. Montoya, C. Tsai, A. Vojvodic, J.K. Nørskov, *Chemsuschem* **8**(13), 2180–2186 (2015)
29. J.G. Howalt, T. Vegge, *Beilstein J. Nanotechnol.* **5**(1), 111–120 (2014)
30. A.B. Höskuldsson, Y. Abghoui, A.B. Gunnarsdóttir, E. Skúlason, *ACS Sustain. Chem. Eng.* **5**(11), 10327–10333 (2017)
31. L.M. Azofra, N. Li, D.R. MacFarlane, C. Sun, *Energy Environ. Sci.* **9**(8), 2545–2549 (2016)
32. Y. Liu, Y. Su, X. Quan, X. Fan, S. Chen, H. Yu, H. Zhao, Y. Zhang, J. Zhao, *ACS Catal.* **8**(2), 1186–1191 (2018)
33. L. Zhang, X. Ji, X. Ren, Y. Ma, X. Shi, Z. Tian, A.M. Asiri, L. Chen, B. Tang, X. Sun, *Adv. Mater.* **30**(28), 1800191 (2018)
34. L. Zhang, X. Ji, X. Ren, Y. Luo, X. Shi, A.M. Asiri, B. Zheng, X. Sun, *ACS Sustain. Chem. Eng.* **6**(8), 9550–9554 (2018)
35. X. Yang, J. Nash, J. Anibal, M. Dunwell, S. Kattel, E. Stavitski, K. Attenkofer, J.G. Chen, Y. Yan, B. Xu, J. Am. Chem. Soc. **140**(41), 13387–13391 (2018)
36. Y. Song, D. Johnson, R. Peng, D.K. Hensley, P.V. Bonnesen, L. Liang, J. Huang, F. Yang, F. Zhang, R. Qiao, A.P. Baddorf, *Sci. Adv.* **4**(4), e1700336 (2018)
37. M. Nazemi, M.A. El-Sayed, *J. Phys. Chem. Lett.* **9**(17), 5160–5166 (2018)
38. Yao, Y., Feng, Q., Zhu, S., Li, J., Yao, Y., Wang, Y.,... & Yuan, X. Z. (2018). *Small Methods*, 1800324
39. J. Ran, J. Zhang, J. Yu, M. Jaroniec, S.Z. Qiao, *Chem. Soc. Rev.* **43**(22), 7787–7812 (2014)
40. L. Xu, Q. Jiang, Z. Xiao, X. Li, J. Huo, S. Wang, L. Dai, *Angew. Chem. Int. Ed.* **55**(17), 5277–5281 (2016)
41. W.J. Ong, L.L. Tan, Y.H. Ng, S.T. Yong, S.P. Chai, *Chem. Rev.* **116**(12), 7159–7329 (2016)
42. A. Fuertes, *Mater. Horizons* **2**(5), 453–461 (2015)
43. S. Cao, J. Low, J. Yu, M. Jaroniec, *Adv. Mater.* **27**(13), 2150–2176 (2015)
44. Y. Zheng, J. Liu, J. Liang, M. Jaroniec, S.Z. Qiao, *Energy Environ. Sci.* **5**(5), 6717–6731 (2012)
45. J. Ran, G. Gao, F.T. Li, T.Y. Ma, A. Du, S.Z. Qiao, *Nat. Commun.* **8**, 13907 (2017)
46. S. Sun, Q. An, W. Wang, L. Zhang, J. Liu, W.A. Goddard III, *J. Mater. Chem. A* **5**(1), 201–209 (2017)
47. H. Li, J. Shang, J. Shi, K. Zhao, L. Zhang, *Nanoscale* **8**(4), 1986–1993 (2016)
48. Y. Bai, L. Ye, T. Chen, L. Wang, X. Shi, X. Zhang, D. Chen, *ACS Appl. Mater. Interfaces* **8**(41), 27661–27668 (2016)
49. H. Hirakawa, M. Hashimoto, Y. Shiraiishi, T. Hirai, *J. Am. Chem. Soc.* **139**(31), 10929–10936 (2017)
50. Y. Zhao, Y. Zhao, G.I. Waterhouse, L. Zheng, X. Cao, F. Teng, L.Z. Wu, C.H. Tung, D. O'Hare, T. Zhang, *Adv. Mater.* **29**(42), 1703828 (2017)
51. G. Dong, W. Ho, C. Wang, *J. Mater. Chem. A* **3**(46), 23435–23441 (2015)
52. N. Zhang, A. Jalil, D. Wu, S. Chen, Y. Liu, C. Gao, W. Ye, Z. Qi, H. Ju, C. Wang, X. Wu, *J. Am. Chem. Soc.* **140**(30), 9434–9443 (2018)
53. J. Yang, Y. Guo, R. Jiang, F. Qin, H. Zhang, W. Lu, J. Wang, J.C. Yu, *J. Am. Chem. Soc.* **140**(27), 8497–8508 (2018)
54. D. Yang, T. Chen, Z. Wang, *J. Mater. Chem. A* **5**(36), 18967–18971 (2017)
55. D. Bao, Q. Zhang, F.L. Meng, H.X. Zhong, M.M. Shi, Y. Zhang, J.M. Yan, Q. Jiang, X.B. Zhang, *Adv. Mater.* **29**(3), 1604799 (2017)
56. M.M. Shi, D. Bao, B.R. Wulan, Y.H. Li, Y.F. Zhang, J.M. Yan, Q. Jiang, *Adv. Mater.* **29**(17), 1606550 (2017)
57. S.J. Li, D. Bao, M.M. Shi, B.R. Wulan, J.M. Yan, Q. Jiang, *Adv. Mater.* **29**(33), 1700001 (2017)
58. Kim, K., Yoo, C.-Y., Kim, J.-N., Yoon, H.C. & Han, J.-I. **163**, F1523–F1526 (2016)
59. N. Furuya, H. Yoshida, *J. Electroanal. Chem. Interfacial Electrochem.* **263**, 171–174 (1989)
60. N. Furuya, H. Yoshida, *J. Electroanal. Chem. Interfacial Electrochem.* **291**, 269–272 (1990)
61. A. Tsuneto, A. Kudo, T. Sakata, *J. Electroanal. Chem.* **367**, 183–188 (1994)
62. Kordali, V., Kyriacou, G. & Lambrou, C. *Chem. Commun.*, 1673–1674 (2000)
63. F. Köleli, T. Röpke, *Appl. Catal. B* **62**, 306–310 (2006)
64. R. Lan, J.T.S. Irvine, S. Tao, *Sci. Rep.* **3**, 1145 (2013)
65. R. Lan, S. Tao, *RSC Adv.* **3**, 18016–18021 (2013)
66. K. Kugler, M. Luhn, J.A. Schramm, K. Rahimi, M. Wessling, *Phys. Chem. Chem. Phys.* **17**, 3768–3782 (2015)
67. K. Kim, N. Lee, C.Y. Yoo, J.N. Kim, H.C. Yoon, J.I. Han, *J. Electrochem. Soc.* **163**(7), F610–F612 (2016)
68. J. Kong, A. Lim, C. Yoon, J.H. Jang, H.C. Ham, J. Han, S. Nam, D. Kim, Y.E. Sung, J. Choi, H.S. Park, *ACS Sustain. Chem. Eng.* **5**(11), 10986–10995 (2017)
69. S. Chen, S. Perathoner, C. Ampelli, C. Mebrahtu, D. Su, G. Centi, *ACS Sustain. Chem. Eng.* **5**(8), 7393–7400 (2017)
70. G.F. Chen, X. Cao, S. Wu, X. Zeng, L.X. Ding, M. Zhu, H. Wang, *J. Am. Chem. Soc.* **139**(29), 9771–9774 (2017)
71. X. Zhao, F. Yin, N. Liu, G. Li, T. Fan, B. Chen, *J. Mater. Sci.* **52**(17), 10175–10185 (2017)
72. S. Chen, S. Perathoner, C. Ampelli, C. Mebrahtu, D. Su, G. Centi, *Angew. Chem. Int. Ed.* **56**(10), 2699–2703 (2017)
73. F. Zhou, L.M. Azofra, M. Ali, M. Kar, A.N. Simonov, C. McDonnell-Worth, C. Sun, X. Zhang, D.R. MacFarlane, *Energy Environ. Sci.* **10**(12), 2516–2520 (2017)
74. H.M. Liu, S.H. Han, Y. Zhao, Y.Y. Zhu, X.L. Tian, J.H. Zeng, J.X. Jiang, B.Y. Xia, Y. Chen, *J. Mater. Chem. A* **6**(7), 3211–3217 (2018)
75. X. Ren, G. Cui, L. Chen, F. Xie, Q. Wei, Z. Tian, X. Sun, *Chem. Commun.* **54**(61), 8474–8477 (2018)
76. X. Zhang, R.-M. Kong, H. Du, L. Xia, F. Qu, *Chem. Commun.* **54**, 5323–5325 (2018)
77. B.L. Sheets, G.G. Botte, *Chem. Commun.* **54**, 4250–4253 (2018)
78. C. Lv, C. Yan, G. Chen, Y. Ding, J. Sun, Y. Zhou, G. Yu, *Angew. Chem.* **130**(21), 6181–6184 (2018)
79. M. Nazemi, S.R. Panikkanvalappil, M.A. El-Sayed, *Nano Energy* **49**, 316–323 (2018)
80. C. Zhang, G. Chen, C. Lv, Y. Yao, Y. Xu, X. Jin, Q. Meng, *ACS Sustain. Chem. Eng.* **6**(9), 11190–11195 (2018)

Submit your manuscript to a SpringerOpen[®] journal and benefit from:

- Convenient online submission
- Rigorous peer review
- Open access: articles freely available online
- High visibility within the field
- Retaining the copyright to your article

Submit your next manuscript at ► [springeropen.com](https://www.springeropen.com)